Bioorg. Med. Chem. 41 (2021) 116217

Contents lists available at ScienceDirect

Bioorganic & Medicinal Chemistry

journal homepage: www.elsevier.com/locate/bmc

A minimally-masked inactive prodrug of panobinostat that is bioorthogonally activated by gold chemistry

Belén Rubio-Ruiz [a,1,*], Ana M. Pérez-López [a,2], Víctor Sebastián [b,c,d], Asier Unciti-Broceta [a,*]

[a] Cancer Research UK Edinburgh Centre, Institute of Genetics & Cancer, University of Edinburgh, Edinburgh, UK
[b] Department of Chemical Engineering, University of Zaragoza, Campus Río Ebro-Edificio I+D, C/ Poeta Mariano Esquillor S/N, 50018 Zaragoza, Spain
[c] Instituto de Nanociencia y Materiales de Aragón (INMA), CSIC-Universidad de Zaragoza, Zaragoza 50009, Spain
[d] Networking Research Center on Bioengineering Biomaterials and Nanomedicine (CIBER- BBN), Madrid, Spain

ARTICLE INFO

Keywords:
Bioorthogonal catalysis
Gold nanoparticles
HDAC inhibitors
Anticancer therapies

ABSTRACT

The recent incorporation of Au chemistry in the bioorthogonal toolbox has opened up new opportunities to deliver biologically independent reactions in living environments. Herein we report that the *O*-propargylation of the hydroxamate group of the potent HDAC inhibitor panobinostat leads to a vast reduction of its anticancer properties (>500-fold). We also show that this novel prodrug is converted back into panobinostat in the presence of Au catalysts in vitro and in cell culture.

1. Introduction

Histone deacetylases (HDCAs) are a family of enzymes involved in the regulation of gene expression through chromatin remodeling via histone deacetylation.[1] This type of enzymes is overexpressed in many human cancers which result in the repression of vital tumor suppressor genes.[2] HDAC inhibitors (HDACi), regarded as "epigenetic modifiers", inhibit cell proliferation and angiogenesis, promote differentiation and induce apoptosis by modulation of the acetylation status of histones and non-histone proteins.[3]

Developed by Novartis, the pan-HDACi panobinostat (**1**) was approved in 2015 for the treatment of adult patients with relapsed and/or refractory multiple myeloma in combination with bortezomib and dexamethasone.[4] With superior activity than its clinical counterparts vorinostat, romidepsin or belinostat, **1** has been enrolled in multiple clinical trials for the treatment of a variety of cancers, including non-small-cell lung carcinoma (NSCLC).[5] However, the clinical outcomes of those studies have not yet reflected the promising results from the preclinical work, which is partly attributed to its limited tolerability. Dose-limiting toxicities such as neutropenia and thrombocytopenia have been associated with **1** treatment due to the modulation of the expression of undesired genomic regions in healthy cells.[6]

Achieving a focalized cytotoxic effect exclusively at the location of the tumour is one of the main challenges in cancer therapy and drug delivery. In this context, the field of bioorthogonal catalysis has opened the possibility to "synthesize" drugs where and when desired, e.g. inside a tumour, using chemistries that cannot be performed by human enzymes. The combined use of implantable devices incorporating nonbiological catalysts (e.g. Pd) together with systemically-administered inactive drug precursors that are only labile to the catalyst of choice has been recently proposed as a bioorthogonally-activated prodrug approach.[7–11] Such a strategy would potentially reduce systemic side effects and, at the same time, enhance treatment efficacy.

The potential use of bioorthogonal catalysis in biomedicine has attracted a number of research groups in recent years into this emerging field, which has resulted in the development of different strategies to deliver the catalyst to the right location[12–14] and in the discovery of different metals and chemistries that can release drugs.[15–18] One of such findings was the discovery of the capacity of gold nanoparticles (Au-NPs) to mediate depropargylation reactions in living environments.[19] The main advantage of this chemistry is the high tolerability of Au, which makes its use ideal for medical applications. Motivated by this, here we report the development of a novel bioorthogonal prodrug of the HDACi panobinostat, which shows high stability and low anti-proliferative activity in cell culture, and that can be activated by Au catalysis.

* Corresponding authors.
E-mail addresses: belenrubio@ugr.es (B. Rubio-Ruiz), asier.ub@ed.ac.uk (A. Unciti-Broceta).
[1] Present address: Pfizer-University of Granada-Andalusian Regional Government Centre for Genomics and Oncological Research (GENYO) and Department of Medicinal and Organic Chemistry, Faculty of Pharmacy, University of Granada, Granada, Spain.
[2] Present address: Institut für Biotechnologie, Technische Universität Berlin, Berlin, Germany.

https://doi.org/10.1016/j.bmc.2021.116217
Received 2 March 2021; Received in revised form 4 May 2021; Accepted 11 May 2021
Available online 15 May 2021

2. Results and discussion

2.1. Design, synthesis and stability in cell culture of novel panobinostat prodrug

As others structurally-related HDACi, the pharmacological activity of **1** fundamentally relies on the capacity of its hydroxamate group to bind bidentately to a Zn^{2+} ion at the catalytic site of class I, II and IV HDACs, forming a five-membered chelate that result in the inhibition of these enzymes.[20] Based on this mechanism of action, several bio-responsive[21–27] and biorthogonal[9,12] prodrugs of HDACi have been previously developed through subtle modifications of the OH of the hydroxamate group. Since the chemical structure of **1** possess different positions susceptible to be alkylated, direct alkylation reactions can lead to multiple products. Thus, we followed the synthetic route shown in the Scheme 1 for the preparation of the *O*-propargylated hydroxamate derivative **2**. Alkylation of commercial *N*-hydroxyphthalimide afforded intermediate **3**. Then, the phthaloyl group was removed by hydrazinolysis and the filtrate treated with a hydrochloric acid solution in diethyl ether to obtain the corresponding salt **4**. In parallel, ester derivative **5** was synthesized by a reductive amination and hydrolyzed into the carboxylic acid using an aqueous solution of NaOH. In the last step, derivative **2** was obtained by a coupling reaction between the *O*-propargylated hydroxylamine **4** and the β-substituted-acrylic acid **6** that was previously activated with a water-soluble carbodiimide.

To corroborate that the chelating properties of **1** were adequately diminished by the introduction of the propargyl moiety, we first performed a colorimetric test with $FeCl_3$. This sensitive method is based on the ability of hydroxamic acids to react with ferric cations forming easily-detected coloured coordination complexes.[28] As a result, compound **1** gave rise to a purple coloration upon the addition of a hydro-alcoholic solution of $FeCl_3$, while compound **2** did not elicit any colour change relative to the negative control (DMSO) (Supplementary material, Fig. S1). Once proved the efficiency of the masking strategy, we were next interested in testing the stability of the new derivative in a cellular environment. Human lung adenocarcinoma A549 cells were treated for 5 days with increasing concentrations of **1** and **2** (0.001–100 μM) and EC_{50} values calculated from the generated 10-point semilog dose–response curves. As observed in Fig. 1, derivate **2** displayed a vast reduction of its antiproliferative properties relative to **1**, resulting in > 500-fold less bioactivity than the parent compound. This not only shows the importance of the free hydroxamate group for the bioactivity of **1**, but also demonstrates stability of the *O*-propargylated hydroxamate group in cell culture. To the best of our knowledge, this is the first reported bioorthogonal prodrug of an HDACi that shows such a wide therapeutic window, which is remarkable given the small size (C_3H_3) and structural simplicity of the masking group.

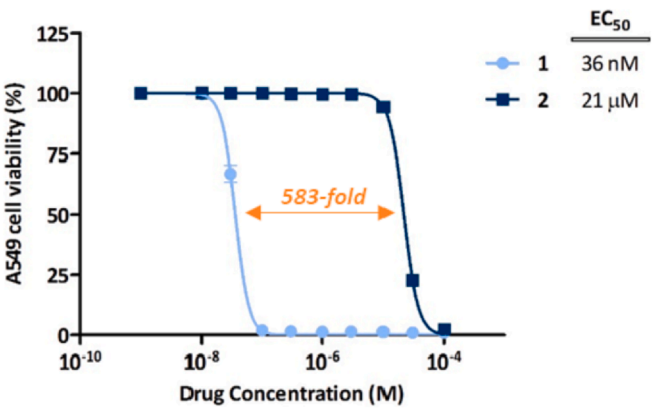

Fig. 1. Dose–response curves for **1** and **2** against A549 cells after 5 days of treatment. Error bars: ± SD from n = 3.

2.2. Preparation and use of biocompatible Au-catalysts

Aiming to avoid the use of toxic reagents, a green methodology was developed to prepare heterogeneous Au-catalysts using trisodium citrate as a biocompatible reducing and stabilising agent. Au-catalysts were prepared by treating amino-functionalized TentaGel® HL resins (Fig. 2a-b), with a diameter of approximately 75 μm, with gold(III) chloride and NaOH in THF at 60 °C for 10 min. Subsequent in-situ reduction with trisodium citrate at room temperature (rt) generated ultra-small sized Au-NPs. The back scattered electron microscopy imaging by SEM shows that Au-NPs (bright contrast) growth homogenously on the resin surface (Fig. 2c). To shed light on the growth of Au-NPs in the internal porous structure of the spherical polystyrene resins, the sample was sectioned with an ultramicrotome and analysed by SEM and TEM. Fig. 2d depicts the cross section of the spherical resin, as well as the locations (center, middle and edge) where high magnification SEM images show a uniform grafting of Au-NPs in the low-crosslinked polystyrene matrix (Fig. 2e-j). The ultramicrotome sectioning enabled to prepare 50 nm thick slices which allow electrons to transmit through the sample under TEM analysis. Fig. 2k-l shows representative TEM Images of Au-NPs located in the resin, edge (Fig. 2k) and centre (Fig. 2-l). The particle size distribution histogram evidenced that the nanocrystallization of Au-NPs is uniform, achieving a narrow particle size distribution 2.8 ± 1.2 nm

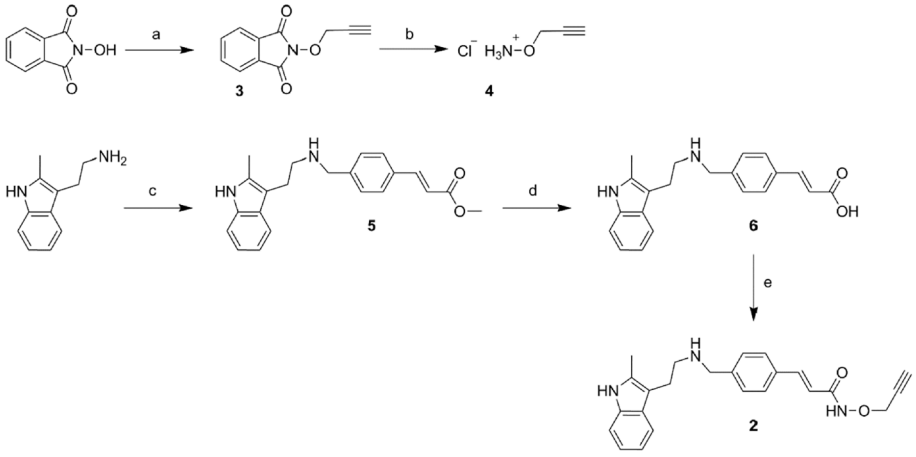

Scheme 1. Synthesis of *O*-alkyl panobinostat derivative **2**. Reagents and conditions: (a) propargyl bromide, NaH, DMF, 70 °C, 24 h, 67%; (b) hydrazine monohydrate, 2 h, rt, HCl in ether, 46% (c) Methyl 4-formylcinnamate, $NaBH_3CN$, DCM/MeOH, rt, overnight, 49%; (d) NaOH, THF/ H_2O, rt, overnight, 70%; (e) EDC, H_2O, rt, then add **4**, 6 h, 27%.

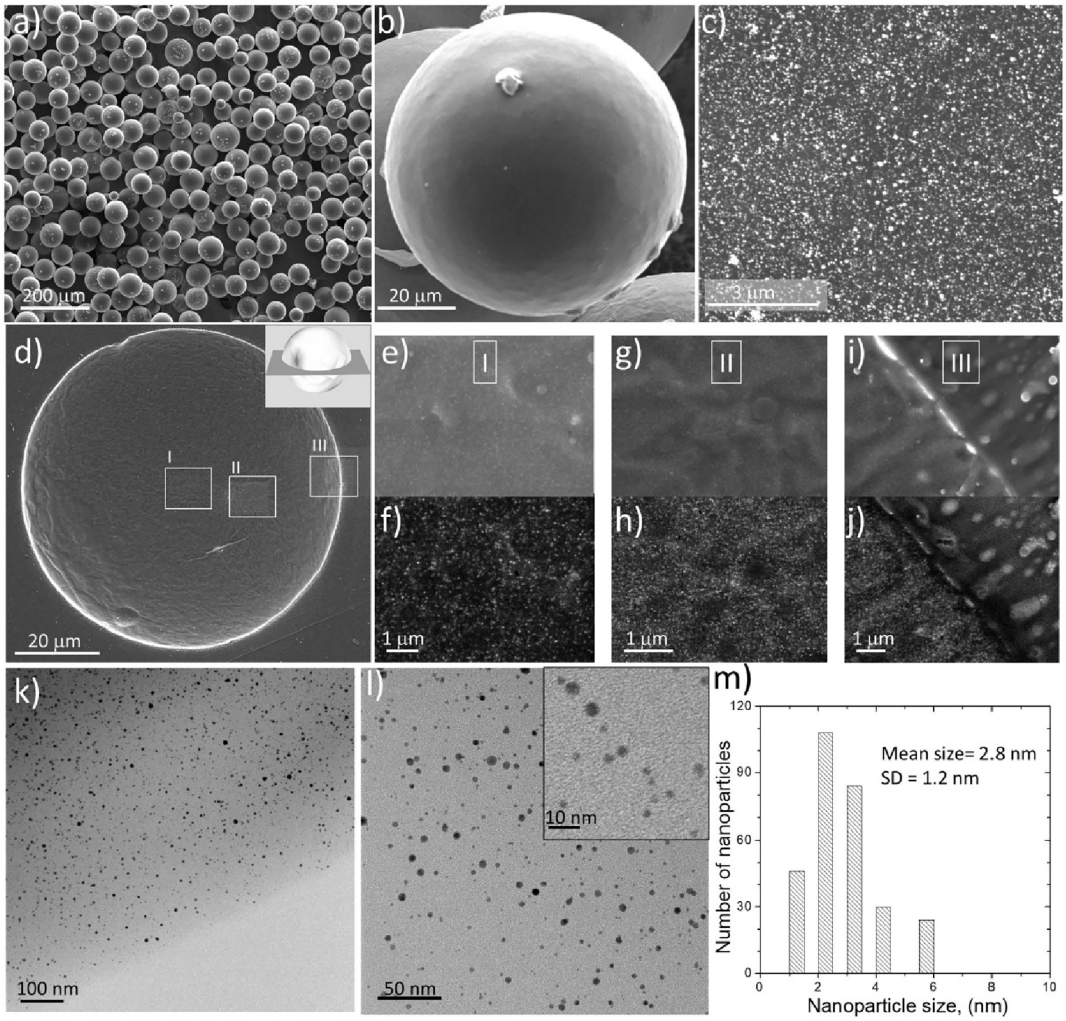

Fig. 2. (A) Scanning electron microscopy images (SEM) of Au-catalysts. (B) Detail image of a spherical Au-resin. (C) Backscattered Electron SEM image of the surface of the Au-resin to observe the Au-NPs. (D) SEM cross section image of an Au-resin. (E, G, I) Secondary Electron SEM images of marked areas I-II-III in panel D. (F, H, J) Backscattered Electron SEM images of marked areas I-II-III in panel D. Location and homogenous distribution of Au-NP are observed throughout a cross-section of an Au-resin. (K, L) TEM images of Au-NPs embedded in the resin. (M) Particle size histogram of Au NPs (n = 292).

(Fig. 2-m). The presence of the metal was also confirmed by ICP-OES, with a 0.12% w/w of Au content.

Next, we tested the catalytic activity of these Au-functionalised devices using a caged rhodamine dye (**7**), which upon deprotection emits bright green fluorescence that can be measured in a spectrofluorometer (see chemical structure in the Supplementary material). To validate them under conditions similar to the ones used in cell assays, Au-catalysts were incubated overnight with a solution of **7** in PBS or PBS supplemented with FBS (10%) at 37 °C and then the reactions crudes analysed. In agreement with prior studies,[19] the Au-catalysed conversion of **7** into **8** was improved in the presence of serum (Supplementary material, Fig. S2). This is important because serum proteins and biogenic thiols can affect negatively the catalytic properties of some catalysts.[13,29]

Due to their size, these devices can be recovered by centrifugation and recycled. Accordingly, we performed a reusability study to test their capacity to activate multiple doses of **7** over time. Although a moderate reduction in activity was observed, Au-catalysts maintained 50% of their catalytic efficiency after 3 consecutive cycles in the presence of serum (Supplementary material, Fig. S2).

Encouraged by the results obtained from the prodye-into-dye conversion assay, we assessed the biocompatibility of these new devices in A549 cells. As expected, Au-catalysts proved to be completely harmless at all concentrations studied and consequently, suitable for bio-orthogonal applications (see Supplementary material).

2.3. Prodrug-into-drug conversion studies

We then studied the capacity of Au-catalysts to convert inactive compound **2** into highly potent HDACi **1** in physiological conditions. Derivative **2** was incubated in PBS at pH = 7.4 and 37 °C and analyzed by LC/MS. Incubation with Au-catalysts under such conditions resulted in a "clean" cleavage of the propargyl group of **2** with no other side products detected (Supplementary material Fig. S3). Of note, when this reaction was performed with Pd-catalysts (data not shown), a complex mix of products was obtained. This result is consistent with previous observations with an *O*-propargylated derivative of vorinostat.[9]

Next, the conversion studies were performed in cell culture, using NSCLC A549 cells. Au-catalysts (1 mg/mL) and **2** (1or 3 µM) were incubated with cells separately (negative controls) or in combination (activation assay) for 5 days. Unmodified **1** (1 or 3 µM) was used as a control (Supplementary material, Fig. S5). Dose-response studies evidenced the efficient generation of the drug in the presence of the catalyst at both concentrations. As expected, no signs of cell death were observed by separately treating the cells with Au-catalysts or prodrug **2**, while a strong cytotoxic effect was induced by the combined treatment of both

reagents. Last, in order to test the durability of the catalyst in culture, we performed an activation study of multiple prodrug doses in A549 cells (Fig. 3). Au-catalysts (1 mg/mL) were placed in semipermeable transwell inserts with 8 μm pore size. After each prodrug-into-drug conversion cycle, the inserts containing Au-catalysts were transferred to freshly seeded plates and incubated again with prodrug **2** (3 μM) for 3 days, which confirmed the reusability of the Au-catalysts in 3 successive cycles.

The results obtained in A549 cells were verified in a second cell line (glioblastoma U87 cells, see Supp. Fig. 6–8).

3. Conclusions

Here we report that the *O*-propargylation of the hydroxamate group of panobinostat generates an inactive derivative that is harmless to cells and can be converted back into cytotoxic panobinostat by Au catalysis. Of note, Pd-catalysts failed to provide the desired product. In addition, we also provide a new "green" method for the generation of solid-supported Au-NPs with an excellent size control that are compatible with bioorthogonal applications.

4. Material and methods

4.1. Chemistry: General conditions

Chemicals were purchased from Fisher Scientific, Sigma-Aldrich or VWR. **1** was purchased from LC Laboratories. Resins were purchased from Rapp Polymere GmbH. NMR spectra were recorded at rt on a 500 MHz Bruker Avance III spectrometer. Chemical shifts are reported in ppm relative to the solvent peak. High Resolution Mass Spectrometry was measured in a Bruker MicrOTOF II. Analytical TLC was performed using Merck TLC Silica gel 60 F_{254} plates and visualized by UV light. Purifications were carried out by flash column chromatography using commercially available silica gel (220–440 mesh, Sigma-Aldrich). Compound used in the biological experiments was > 95% pure, as measured by UPLC using a Waters BEH C18 column 50 × 2.4 mm, 1.7 μm; 60 °C and an UV–Vis 254 nm detector. Method: eluent A: water and TFA (0.1%); eluent B: acetonitrile; flow rate = 0.4 mL/min; A/B = 95:5 to 5:95 in 2.5 min, isocratic 0.5 min, 5:95 to 95:5 in 1 min. Stock solutions (100 mM) were prepared in DMSO.

4.2. Synthetic procedures of intermediates compounds

4.2.1. Synthesis of N-(propargyloxy)phthalimide (3)

N-(propargyloxy)phthalimide (**3**) was synthesised following the procedure previously described.[30] Briefly, *N*-hydroxyphthalimide (1000 mg, 6.1 mmol) was dissolved in dry dimethylformamide (DMF) under a nitrogen atmosphere. The *N*-hydroxyphthalimide in DMF was then added to NaH (7.3 mmol) suspended in DMF under an N_2 atmosphere, yielding a red opaque solution. Then, propargyl bromide (12.2 mmol) in DMF was added dropwise. The reaction mixture was heated to 70 °C and stirred for 24 h. The DMF solvent was removed at reduced pressure, the residue dissolved in chloroform ($CHCl_3$) and washed with of H_2O, $NaHSO_3$/ Na_2CO_3 (aq). The $CHCl_3$ layer was dried over anhydrous Na_2SO_4, evaporated under reduced pressure and recrystallized from hot ethanol giving rise a light-brown solid (816 mg, 67%). NMR characterization matches previously reported.[31]

4.2.2. Synthesis of O-(propargyl)hydroxylamine hydrochloride (4)

Compound **3** (1.0 mmol) was dissolved in diethyl ether (6 mL) and treated with hydrazine monohydrate (2.0 mmol). The reaction mixture was stirred for 2 h at rt Then, the solid residue was removed by filtration and HCl in ether (2 M, 4 mL) added to the filtrate with continuous stirring. The reaction was stirred for an additional 2 h and the resulting solid filtered and dried yielding **4** as a light yellow-solid (44 mg, 46%). Characterization data matches previously reported data.[32]

4.2.3. Synthesis of (E)-methyl 3-(4-{[2-(2-methyl-1H-indol-3-yl) ethylamino]methyl}phenyl)acrylate (5)

(*E*)-Methyl 3-(4-{[2-(2-methyl-1*H*-indol-3-yl)ethylamino]methyl} phenyl)acrylate (**5**) was synthesised according to literature procedure yielding an orange-brown solid (975 mg, 49%). Characterization data matches previously reported data.[33]

4.2.4. Synthesis of (E)-3-(4-{[2-(2-methyl-1H-indol-3-yl)ethylamino] methyl}phenyl)acrylic acid (6)

To a solution of **5** (140 mg, 0.4 mmol) in THF/ H_2O (1:5; 2, 5 mL) was added dropwise an aq solution of NaOH 1 N (0.5 mL). The resulting mixture was stirred at rt overnight and then acidified using aq solution of HCl 3 N. The resulting precipitate was filtered, thoroughly washed with CH_3CN, and dried *in vacuo* to give rise an off-white solid (94 mg, 70%). NMR characterization matches previously reported.[34]

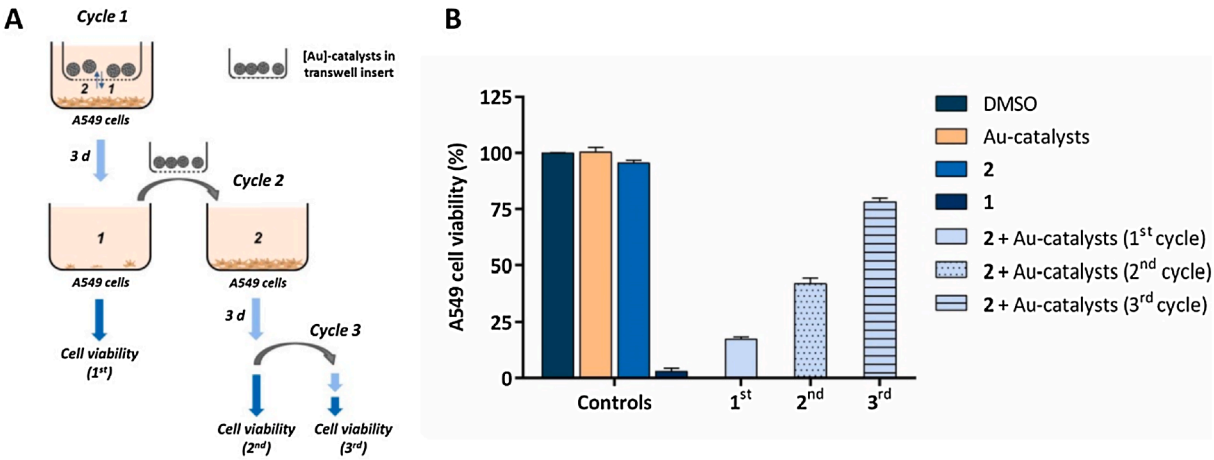

Fig. 3. (A) Activation study of multiple prodrug doses in A549 cancer cell culture. (B) Cell viability analysis of prodrug **2** activation cycles (labelled as 1st, 2nd and 3rd). Prodrug activation assay: Au-catalysts + **2** (light blue). Negative controls: DMSO (untreated cells, dark green); Au-catalysts (orange); and prodrug **2** (blue). Positive control: **1** (dark blue). Error bars: ± SD from n = 3. (For interpretation of the references to colour in this figure legend, the reader is referred to the web version of this article.)

4.3. Synthetic procedure and characterization of prodrug **2**

6 (40 mg, 0.1 mmol) and **4** (0.2 mmol) were added to a 25 mL round-bottom flask and partially dissolved in distilled water (1 mL). *N*-(3-Dimethylaminopropyl)-*N*′-ethylcarbodiimide hydrochloride (0.4 mmol) was then added to the mixture in one portion. The pH was monitored and adjusted to 4.5 with a NaOH and / or HCl aqueous solution (1 M). The reaction was stirred for 6 h at rt and constant pH (4.5). Water was removed under reduced pressure, and crude suspended in acetonitrile and vacuum filtered. Solution was purified by semi-preparative TLC eluting with DCM:MeOH/7:3 giving rise a light-yellow solid (12 mg, 27%). **^{1}H NMR** (500 MHz, DMF) δ 11.42 (bs, 1H), 10.69 (s, 1H), 7.54 (d, J = 7.4 Hz, 2H), 7.49 (d, J = 15.9 Hz, 1H), 7.38 (dd, J = 14.0, 7.9 Hz, 3H), 7.21 (dt, J = 8.0, 0.8 Hz, 1H), 6.96 (ddd, J = 8.1, 7.1, 1.2 Hz, 1H), 6.90 (ddd, J = 8.0, 7.1, 1.1 Hz, 1H), 6.44 (d, J = 15.0 Hz, 1H), 4.54 (d, J = 2.4 Hz, 2H), 3.85 (s, 2H), 3.61 (t, J = 2.3 Hz, 1H), 2.83 (m, 2H), 2.72 (m, 2H), 2.30 (s, 3H). **^{13}C NMR** (126 MHz, DMSO) δ 162.9, 139.5, 135.2, 133.5, 132.0, 129.0, 128.2 (x2), 127.6 (x2), 119.9, 118.1 (x2), 117.9, 117.3, 110.4, 107.3, 78.9, 78.6, 62.5, 51.7, 48.9, 23.4, 11.2. **HRMS (ESI)** *m/z* $[M + H]^+$ calculated for $C_{24}H_{26}O_2N_3$, 388.2019; found, 388.2018. UPLC purity: > 95%; Rt: 1.496 min.

4.4. Synthesis and characterization of Au-catalysts

4.4.1. Synthetic procedure

TentaGel® HL NH_2 resins (250 mg, 0.4–0.6 mmol/g, particle size 75 μm) were added into a 25 mL Biotage microwave vial and suspended in THF (2.5 mL). A solution of gold(III) chloride hydrate (120 mg, 0.4 mmol) in distilled water (500 μL) was basified with a 1 M NaOH aqueous solution (11 μL). This freshly prepared solution was immediately added to the suspended resins and heated to 60 °C under stirring for 10 min. The mixture was then stirred at rt for additional 2 h. Subsequently, the solvents were filtered and the resins washed with DMF (3 × 10 mL), DCM (3 × 10 mL) and methanol (3 × 10 mL). A solution of trisodium citrate in distilled water (200 mM, 5 mL) was prepared. This solution was added to the gold(III)-treated resins and bubbled with a N_2 flow at rt for 10 min. Then, resins were stirred for 1 h at rt in a rotatory wheel. The solvents were then filtered off and the resins washed with water (1 × 10 mL), methanol (3 × 10 mL) and DCM (3 × 10 mL). The solvents were then filtered and resins were dried in an oven at 40 °C for 24 h.

4.4.2. Electron microscopy analyses

Morphological analysis of Au-catalysts was carried out by Scanning Electron Microscopy (SEM, Inspect F50; FEI, Eindhoven, the Netherlands) at the LMA-INA-Universidad Zaragoza facilities operated at 10–15 kV. To analyze the cross section of the Au-catalysts, it was required to infiltrate and embed them in a liquid epoxy resin. After curing the resin block, it was sectioned with an Ultramicrotome (Leica EM UC7) equipped with a diamond knife. Sections of 50–70 nm thickness were collected on a copper grid (formvar-200 mesh) coated with carbon film, and allowed to dry in air. The cross-section of the Au-catalysts, that was embedded in the resin block, was analyzed to study the Au nanoparticles dispersion using both Back Scattering Electron and secondary electron Detectors. Transmission Electron Microscopy observations were carried out at using a FEI Tecnai F20 operating at 200 kV.

4.5. Au-catalysed deprotection of probe **7** and reusability of Au-catalysts

Prodye **7** was synthesised as previously reported.[7] Au-catalysts (1 mg) were added to a 1 mL solution of reagent **7** (100 μM) in PBS or PBS supplemented with 10% Fetal Bovine Serum (FBS). The mixtures were shaken at 1,200 rpm and 37 °C in a Thermomixer and reactions monitored at 16 h by fluorescence in a PerkinElmer Victor multilabel reader (excitation filter at 480 nm and emissions filter at 535 nm). Au-catalysts were recovered by centrifugation (13,000 rpm, 5 min) and washed with distilled water. A fresh solution of **7** at 100 μM in PBS or 10% FBS in PBS was added to the Au-catalysts, the mixtures shaken at 1,200 rpm and 37 °C, and fluorescence measured at 16 h as described above. This cycle was repeated 2 times.

4.6. Au-mediated deprotection of prodrug **2** at physiological conditions

Prodrug **2** (200 μM) was dissolved in PBS (1 mL) with 1 mg of Au-catalysts and shaken at 1,200 rpm and 37 °C in a Thermomixer. Reaction crudes were monitored at 24 and 48 h by LCMS/MS (Agilent 1200) using a micrOTOF II detector. LCMS/MS method: eluent A: water and formic acid (0.1%); eluent B: acetonitrile and formic acid (0.1%); A/B = 95:5 isocratic 0.5 min, 95:5 to 0:100 in 4.5 min, isocratic 2 min, 0:100 to 95:5 in 0.5 min, and isocratic 2.5 min (flow = 0.2 mL / min).

4.7. Cell culture

Human lung adenocarcinoma A549 cells and human glioblastoma U87 cells were cultured in Dulbecco's Modified Eagle Media (DMEM) supplemented with serum (10% FBS) and L-glutamine (2 mM) and incubated in a tissue culture incubator at 37 °C and 5% CO_2.

4.8. Biocompatibility of Au-catalysts

Biocompatibility of Au-catalysts was tested by performing dose-response studies in A549 and U87 cells. Cells were seeded in a 96-well plate format (at 1,500 cells/well for A549 and 2,000 cells/well for U87) and incubated for 48 h before treatment. Each well was then replaced with fresh media containing Au-catalysts (0.8, 1.0, 1.2 and 1.4 mg/mL) and incubated for 5 days. Untreated cells were incubated with DMEM media. Experiments were performed in triplicates. PrestoBlue™ cell viability reagent (10% v/v) was added to each well and the plate incubated for 90 min. Fluorescence emission was detected using a PerkinElmer Victor multilabel reader (excitation filter at 540 nm and emissions filter at 590 nm). All conditions were normalized to the untreated cells (100%).

4.9. Cytotoxicity study: Drug vs prodrug

Antiproliferative activity of **1** and *O*-propargylated HDAC derivative **2** were compared by performing dose–response studies in A549 and U87 cells. Cells were seeded as described above and incubated for 48 h before treatment. Each well was then replaced with fresh media, containing compounds (100 μM-0.01 μM) and incubated for 5 days. Untreated cells were incubated with DMSO (0.1% v/v). Experiments were performed in triplicates. PrestoBlue™ cell viability reagent (10% v/v) was added to each well and the plate incubated for 90 min. Fluorescence emission was detected and results normalized as described above.

4.10. Au-mediated activation of prodrug **2** in cell culture

A549 and U87 cells were plated as described above. Each well was then replaced with fresh media containing: Au-catalysts (0.8 mg/mL for U87 cells and 1 mg/mL for A549); **1** (positive control: 10 μM, 3 μM or 1 μM); **2** (10 μM, 3 μM or 1 μM) or a combination of Au-catalysts + **2** (10 μM, 3 μM or 1 μM). All experiments, including the untreated cells, contained 0.1% v/v of DMSO and were performed in triplicates. Cells were incubated with drugs for 5 days. PrestoBlue™ cell viability reagent (10% v/v) was added to each well and the plates were incubated for 90 min. Fluorescence emission was detected and results normalized as described above.

4.11. Multidose prodrug activation study in cancer cell culture

A549 cells were seeded in a 24-well plate format (at 2 × 10^4 cells / well) and incubated for 24 h before treatment. Each well was then

replaced with fresh media containing: Au-catalysts (1 mg/mL), **1** (3 μM), **2** (3 μM) or a combination of **2** and Au-catalysts (1 mg/mL). To facilitate the transferring of the Au-catalysts after each prodrug activation cycle, the Au-catalysts were placed in semipermeable (8 μm pore size) Sarstedt transwell inserts. Cell viability was determined, as described above, after 3 days of incubation. Before adding the PrestoBlue reagent, the inserts containing the Au-catalysts were moved to a previously seeded 24-well plate and incubated for additional 3 days with fresh media with or without **2** (3 μM). This process was performed twice. All experiments, including the untreated cells, contained 0.1% v/v of DMSO and were performed in triplicates. All conditions were normalized to the untreated cells (100%) as described above.

Declaration of Competing Interest

The authors declare that they have no known competing financial interests or personal relationships that could have appeared to influence the work reported in this paper.

Acknowledgements

We gratefully acknowledge financial support from EPSRC (EP/N021134/1 and EP/S010289/1). B.R.-R. thanks the EC (grant no. H2020-MSCA-IF-2014-658833). V.S. acknowledges the financial support of Ministerio de Ciencia, Innovación y Universidades, Programa Retos Investigación, Proyecto REF: RTI2018-099019-A-I00.

Appendix A. Supplementary material

Supplementary data to this article can be found online at https://doi.org/10.1016/j.bmc.2021.116217.

References

1 Cheng Y, He C, Wang M, et al. Targeting epigenetic regulators for cancer therapy: mechanisms and advances in clinical trials. *Signal Transduct Target Ther*. 2019;4:62. https://doi.org/10.1038/s41392-019-0095-0.
2 Glozak MA, Seto E. Histone deacetylases and cancer. *Oncogene*. 2007;26:5420–5432. https://doi.org/10.1038/sj.onc.1210610.
3 Falkenberg KJ, Johnstone RW. Histone deacetylases and their inhibitors in cancer, neurological diseases and immune disorders. *Nat Rev Drug Discov*. 2014;13:673–691. https://doi.org/10.1038/nrd4360.
4 Garnock-Jones KP. Panobinostat: first global approval. *Drugs*. 2015;75:695–704. https://doi.org/10.1007/s40265-015-0388-8.
5 Atadja P. Development of the pan-DAC inhibitor panobinostat (LBH589): successes and challenges. *Cancer Lett*. 2009;280:233–241. https://doi.org/10.1016/j.canlet.2009.02.019.
6 Guha M. HDAC inhibitors still need a home run, despite recent approval. *Nat Rev Drug Discov*. 2015;14:225–226. https://doi.org/10.1038/nrd4583.
7 Weiss JT, Dawson JC, Macleod KG, et al. Extracellular palladium-catalysed dealkylation of 5-fluoro-1-propargyl-uracil as a bioorthogonally activated prodrug approach. *Nat Commun*. 2014;5:3277. https://doi.org/10.1038/ncomms4277.
8 Weiss JT, Dawson JC, Fraser C, et al. Development and bioorthogonal activation of palladium-labile prodrugs of gemcitabine. *J Med Chem*. 2014;57:5395–5404. https://doi.org/10.1021/jm500531z.
9 Rubio-Ruiz B, Weiss JT, Unciti-Broceta A. Efficient palladium-triggered release of vorinostat from a bioorthogonal precursor. *J Med Chem*. 2016;59:9974–9980. https://doi.org/10.1021/acs.jmedchem.6b01426.
10 Bray TL, Salji M, Brombin A, et al. Bright insights into palladium-triggered local chemotherapy. *Chem Sci*. 2018;9:7354–7361. https://doi.org/10.1039/c8sc02291g.
11 Pérez-López AM, Rubio-Ruiz B, Valero T, et al. Bioorthogonal uncaging of cytotoxic paclitaxel through Pd nanosheet-hydrogel frameworks. *J Med Chem*. 2020;63:9650–9659. https://doi.org/10.1021/acs.jmedchem.0c00781.
12 Sancho-Albero M, Rubio-Ruiz B, Pérez-López AM, et al. Cancer-derived exosomes loaded with ultrathin palladium nanosheets for targeted bioorthogonal catalysis. *Nat Catal*. 2019;2:864–872. https://doi.org/10.1038/s41929-019-0333-4.
13 Eda S, Nasibullin I, Vong K, et al. Biocompatibility and therapeutic potential of glycosylated albumin artificial metalloenzymes. *Nat Catal*. 2019;2:780–792. https://doi.org/10.1038/s41929-019-0317-4, 2019/09/01.
14 Du Z, Liu C, Song H, et al. Neutrophil-membrane-directed bioorthogonal synthesis of inflammation-targeting chiral drugs. *Chem*. 2020,;6:2060–2072. https://doi.org/10.1016/j.chempr.2020.06.002, 2020/08/06/.
15 Tsubokura K, Vong KK, Pradipta AR, et al. In Vivo Gold Complex Catalysis within Live Mice. *Angew Chem Int Ed Engl*. 2017;56:3579–3584. https://doi.org/10.1002/anie.201610273.
16 Clavadetscher J, Hoffmann S, Lilienkampf A, et al. Copper Catalysis in Living Systems and In Situ Drug Synthesis. *Angew Chem Int Ed Engl*. 2016;55:15662–15666. https://doi.org/10.1002/anie.201609837.
17 Oliveira BL, Stenton BJ, Unnikrishnan VB, et al. Platinum-Triggered Bond-Cleavage of Pentynoyl Amide and. *J Am Chem Soc*. 2020;142:10869–10880. https://doi.org/10.1021/jacs.0c01622.
18 Sabatino V, Rebelein JG, Ward TR. "Close-to-Release": spontaneous bioorthogonal uncaging resulting from ring-closing metathesis. *J Am Chem Soc*. 2019;141:17048–17052. https://doi.org/10.1021/jacs.9b07193.
19 Pérez-López AM, Rubio-Ruiz B, Sebastián V, et al. Gold-triggered uncaging chemistry in living systems. *Angew Chem Int Ed Engl*. 2017;56:12548–12552. https://doi.org/10.1002/anie.201705609.
20 Hai Y, Christianson DW. Histone deacetylase 6 structure and molecular basis of catalysis and inhibition. *Nat Chem Biol*. 2016;12:741–747. https://doi.org/10.1038/nchembio.2134.
21 Thomas M, Rivault F, Tranoy-Opalinski I, Roche J, Gesson JP, Papot S. Synthesis and biological evaluation of the suberoylanilide hydroxamic acid (SAHA) beta-glucuronide and beta-galactoside for application in selective prodrug chemotherapy. *Bioorg Med Chem Lett*. 2007;17:983–986. https://doi.org/10.1016/j.bmcl.2006.11.042.
22 Li J, Zhu Y, Xie M, Zhang Q, Du W. Design, synthesis, and biological evaluation of target water-soluble hydroxamic acid-based HDACi derivatives as prodrugs. *Chem Biol Drug Des*. 2019;94:1760–1767. https://doi.org/10.1111/cbdd.13577.
23 Liao Y, Xu L, Ou S, et al. *ACS Med Chem Lett*. 2018;9:635–640. https://doi.org/10.1021/acsmedchemlett.8b00057.
24 Bhagat SD, Singh U, Mishra RK, Srivastava A. An endogenous Reactive Oxygen Species (ROS)-activated histone deacetylase inhibitor prodrug for cancer chemotherapy. *ChemMedChem*. 2018;13:2073–2079. https://doi.org/10.1002/cmdc.201800367.
25 Zheng S, Guo S, Zhong Q, et al. Biocompatible boron-containing prodrugs of belinostat for the potential treatment of solid tumors. *ACS Med Chem Lett*. 2018;9:149–154. https://doi.org/10.1021/acsmedchemlett.7b00504.
26 Daniel KB, Sullivan ED, Chen Y, et al. Dual-mode HDAC prodrug for covalent modification and subsequent inhibitor release. *J Med Chem*. 2015;58:4812–4821. https://doi.org/10.1021/acs.jmedchem.5b00539.
27 Calder EDD, Skwarska A, Sneddon D, et al. Hypoxia-activated pro-drugs of the KDAC inhibitor vorinostat (SAHA), 131170 *Tetrahedron*. 2020;76. https://doi.org/10.1016/j.tet.2020.131170.
28 Codd R. Traversing the coordination chemistry and chemical biology of hydroxamic acids. *Coord Chem Rev*. 2008;252:1387–1408. https://doi.org/10.1016/j.ccr.2007.08.001.
29 Martínez-Calvo M, Couceiro JR, Destito P, Rodríguez J, Mosquera J, Mascareñas JL. Intracellular deprotection reactions mediated by palladium complexes equipped with designed phosphine ligands. *ACS Catal*. 2018;8:6055–6061. https://doi.org/10.1021/acscatal.8b01606.
30 High A, Prior T, Bell RA, Rangachari PK. Probing the "active site" of diamine oxidase: structure-activity relations for histamine potentiation by O-alkylhydroxylamines on colonic epithelium. *J Pharmacol Exp Ther*. 1999;288:490–501.
31 Kim JN, Kim KM, Ryu EK. Improved Synthesis of N-Alkoxyphthalimides. 1992; 22:1427–1432. doi:10.1080/00397919208021609.
32 Tecle H, Barrett SD, Lauffer DJ, et al. Design and synthesis of m1-selective muscarinic agonists: (R)-(-)-(Z)-1-Azabicyclo[2.2.1]heptan-3-one, O-(3-(3'-methoxyphenyl)-2-propynyl)oxime maleate (CI-1017), a functionally m1-selective muscarinic agonist. *J Med Chem*. 1998;41:2524–2536. https://doi.org/10.1021/jm960683m.
33 Wang H, Yu N, Chen D, et al. Discovery of (2E)-3-{2-butyl-1-[2-(diethylamino) ethyl]-1H-benzimidazol-5-yl}-N-hydroxyacrylamide (SB939), an orally active histone deacetylase inhibitor with a superior preclinical profile. *J Med Chem*. 2011;54:4694–4720. https://doi.org/10.1021/jm2003552.
34 Li X, Jiang Y, Peterson YK, et al. Design of hydrazide-bearing HDACIs based on panobinostat and their p53 and FLT3-ITD dependency in antileukemia activity. *J Med Chem*. 2020;63:5501–5525. https://doi.org/10.1021/acs.jmedchem.0c00442.